

# Supporting Information

## Lotus Seedpod Inspiration: Particle-Nested Double-Inverse- Opal Film with Fast and Reversible Structural Color Switching for Information Security

Changtong Zhou, Yong Qi, Shufen Zhang\*, Wenbin Niu, Suli Wu, Wei Ma, and Bingtao Tang

State Key Laboratory of Fine Chemicals, Dalian University of Technology, Dalian 116024, China

\*E-mail: zhangshf@dlut.edu.cn

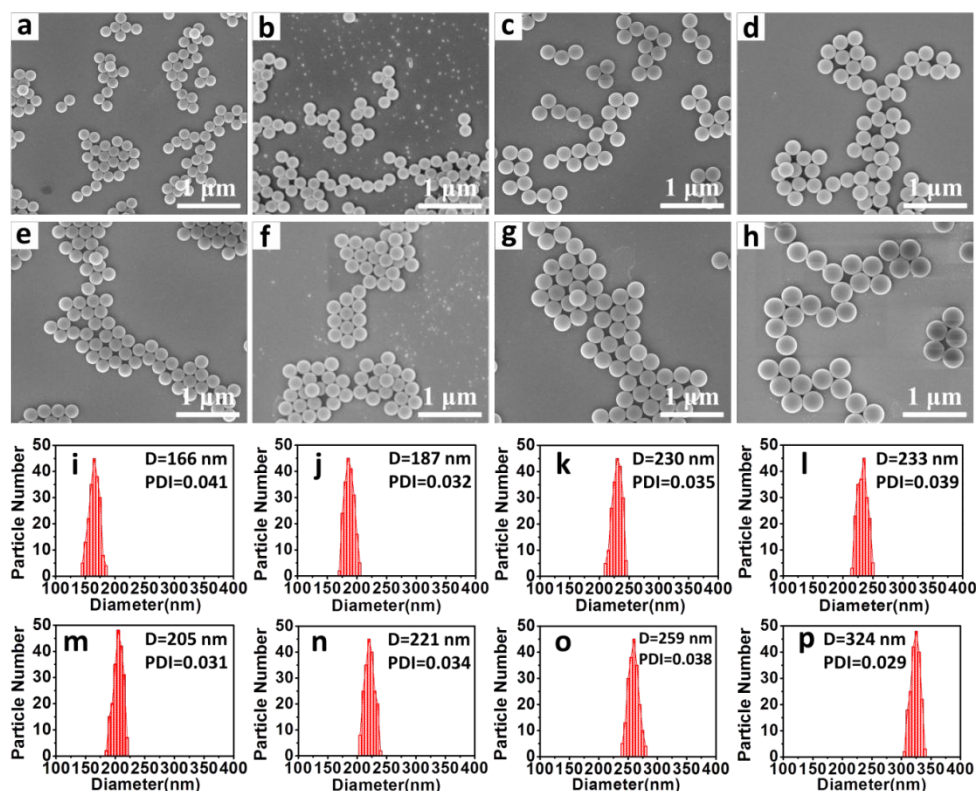


**Figure S1.** SEM images of the prepared PS microspheres and PS@SiO<sub>2</sub> core-shell microspheres. Particle size distribution diagrams of obtained microspheres via counting 200 nanospheres in the corresponding SEM images (a-h). The PDI and D in the figures in (i-p) represent the particle size distribution index and average particle size, respectively.

**Table S1.** Diameters and Zeta-potential of prepared microspheres.

Sample	Size (nm) <sup>a</sup>	PDI <sup>b</sup>	Zeta potential (mV) <sup>c</sup>
PS	166	0.041	-43.7
PS	187	0.032	-48.5
PS	230	0.035	-45.6
PS	233	0.039	-49.8
PS@SiO <sub>2</sub>	205	0.031	-39.2
PS@SiO <sub>2</sub>	221	0.034	-46.3
PS@SiO <sub>2</sub>	259	0.038	-42.5
PS@SiO <sub>2</sub>	324	0.029	-47.4

a: The particle diameters of prepared colloidal microspheres were obtained by counting 200 microspheres in the corresponding SEM images. b and c: Corresponding PDI and Zeta-potential of prepared microspheres were characterized by Dynamic Light Scattering.

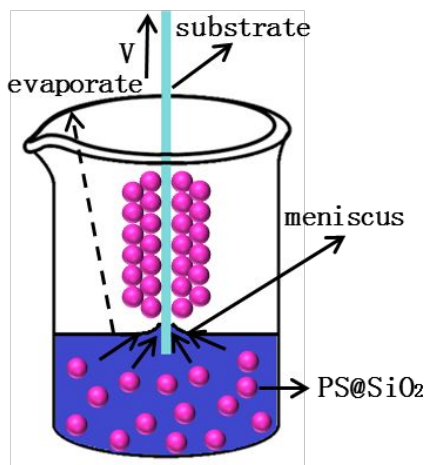


**Figure S2.** Schematic illustration of the dip-coating method.

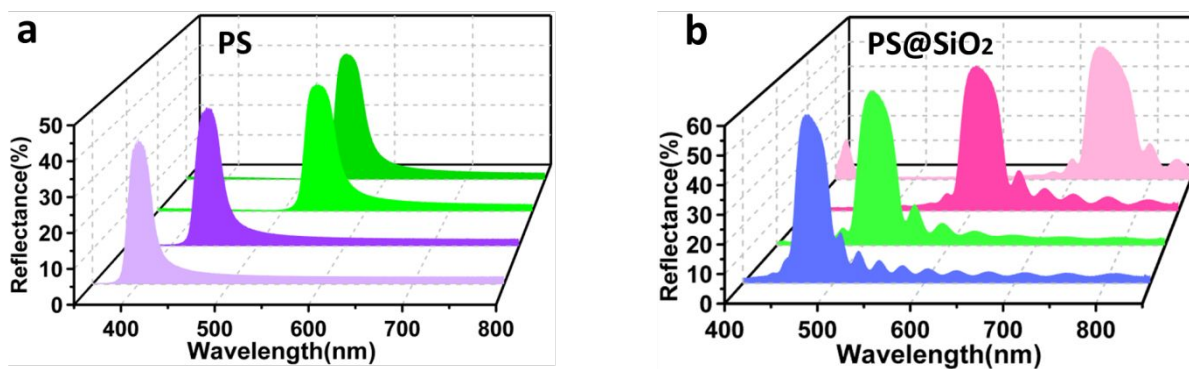


**Figure S3.** Reflection spectra of prepared PC templates (a, PS; b, PS@SiO<sub>2</sub>).

Based on Bragg-Snell's law<sup>1</sup>, the PBG of FCC structured PS PCs could be theoretically calculated as:

$$\lambda_{\max} = 1.633D(n_{\text{avg}}^2 - \sin^2\theta)^{1/2} \quad (1)$$

$$n_{\text{avg}}^2 = 0.74 \times n_{\text{PS}}^2 + 0.26 \times n_{\text{air}}^2 \quad (2)$$

Where  $\lambda_{\max}$  represents the maximum reflected wavelength,  $D$  is the diameter of PS microspheres,  $n_{\text{avg}}$  represents the effective refractive index,  $\theta$  is the incident angle; here  $n_{\text{PS}} = 1.59$  and  $n_{\text{air}} = 1.0$ . Through a simple formula transformation, the theoretical diameter of the prepared PS microspheres can be calculated by the corresponding PBGs based on the following formula:

$$D = \lambda_{\max} / [1.63 \times (2.13 - \sin^2\theta)^{1/2}] \quad (3)$$

For FCC structured PS@SiO<sub>2</sub> PCs, the PBG of could be theoretically calculated based on the following formul<sup>2</sup>:

$$\lambda_{\max} = 1.633D(n_{\text{avg}}^2 - \sin^2\theta)^{1/2} \quad (1)$$

$$n_{\text{avg}}^2 = 0.74 \times n_{\text{core-shell}}^2 + 0.26 \times n_{\text{air}}^2 \quad (4)$$

$$n_{\text{core-shell}} = n_{\text{core}} X_{\text{core}} + n_{\text{shell}} X_{\text{shell}} \quad (5)$$

Where  $\lambda_{\max}$  is the maximum reflected wavelength,  $D$  represents the diameter of PS@SiO<sub>2</sub> core-shell microspheres,  $n_{\text{avg}}$  is the effective refractive index,  $\theta$  is the incident angle; here  $n_{\text{core}}$  and  $n_{\text{shell}}$  are the refractive indexes of each component,  $n_{\text{core}} = n_{\text{PS}} = 1.59$ ,  $n_{\text{shell}} = n_{\text{silica}} = 1.46$ ,

and  $n_{\text{air}} = 1.0$ ;  $X_{\text{core}}$  and  $X_{\text{shell}}$  are the corresponding volume fractions in the PS@SiO<sub>2</sub> core-shell microspheres, respectively. The theoretical diameter of the prepared PS@SiO<sub>2</sub> core-shell microspheres can be calculated by the corresponding PBGs based on the above formulas.

**Table S2.** The diameter of the PS@SiO<sub>2</sub> microspheres (theoretical and practical)

	$\lambda_{\text{max}}$ (nm)	$\theta$ (°)	Theoretical D (nm)	Practical D (nm)
PS	400	5	168	166
PS	441	5	185	187
PS	540	5	227	230
PS	552	5	232	233
PS@SiO <sub>2</sub>	471	5	204	205
PS@SiO <sub>2</sub>	509	5	220	221
PS@SiO <sub>2</sub>	605	5	260	259
PS@SiO <sub>2</sub>	733	5	322	324

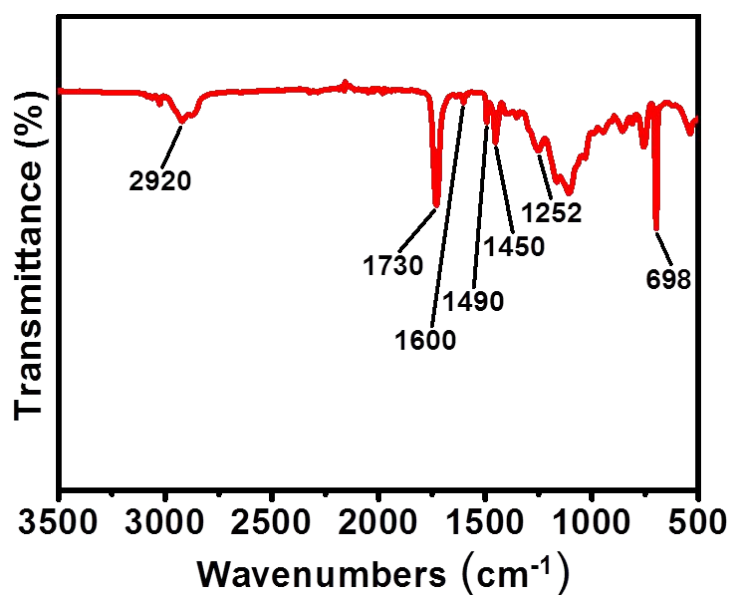


**Figure S4.** FT-IR spectra of the obtained DIOPC film.

PS: 2920  $\text{cm}^{-1}$  ( $\nu$  C-H aliphatic); 1600, 1490, and 1450  $\text{cm}^{-1}$  ( $\nu$  C-C framework of the benzene ring), 698  $\text{cm}^{-1}$  ( $\delta$  single replace of Benzene). Polymer backbone: 1730  $\text{cm}^{-1}$  ( $\nu$  C=O) and 1252  $\text{cm}^{-1}$  ( $\nu$  C-O-C).

**Table S3.** Physical parameters of the liquids used to verify the infiltration response of the patterned sample from nonwetted to wetted states.

Name	Molecular formula	Refractive index	Surface tension (mN/m)
Water	H <sub>2</sub> O	1.33	72.8
Formamid	HCONH <sub>2</sub>	1.45	58.2
Diiodomethane	CH <sub>2</sub> I <sub>2</sub>	1.74	50.8
Ethanol	C <sub>2</sub> H <sub>5</sub> OH	1.36	22.1

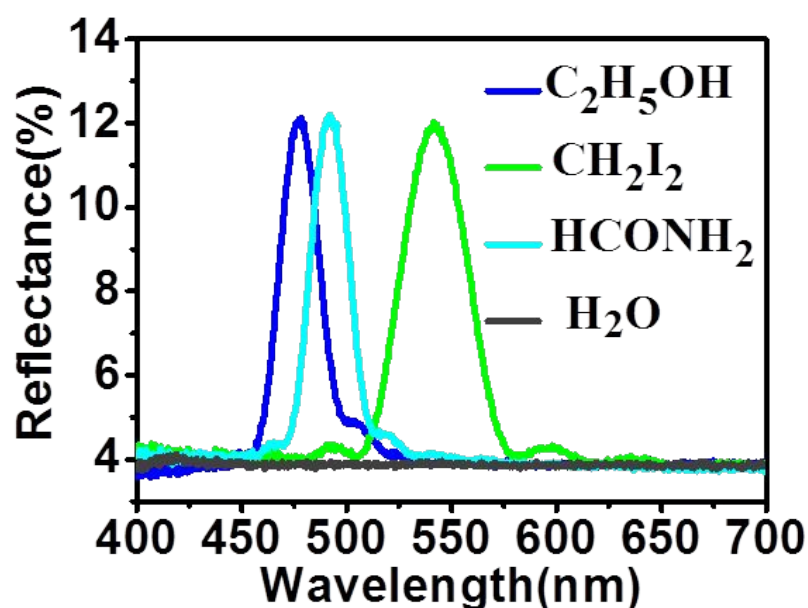


**Figure S5.** Corresponding reflection spectra of Figure 2d.

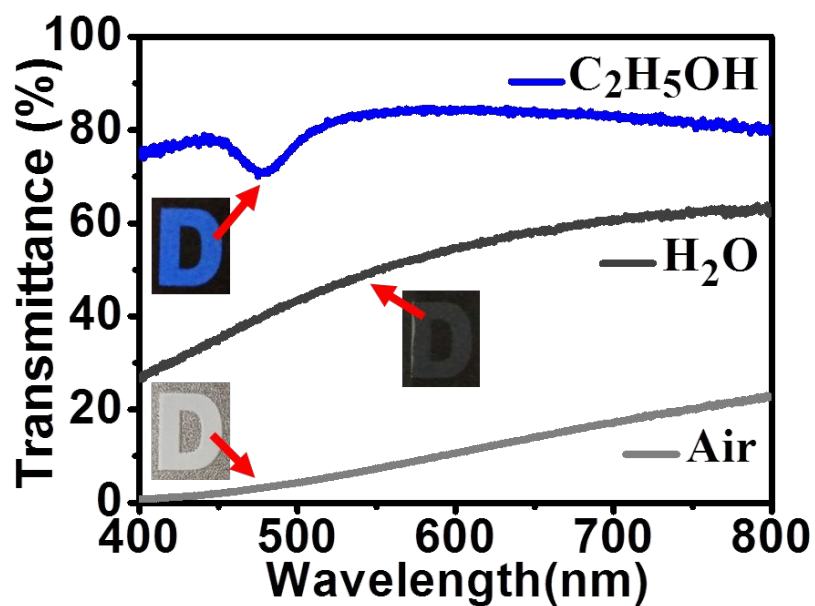


**Figure S6.** Transmission spectra of the prepared patterned DIOPC film with a letter “D” in the air or wiped with water or ethanol.

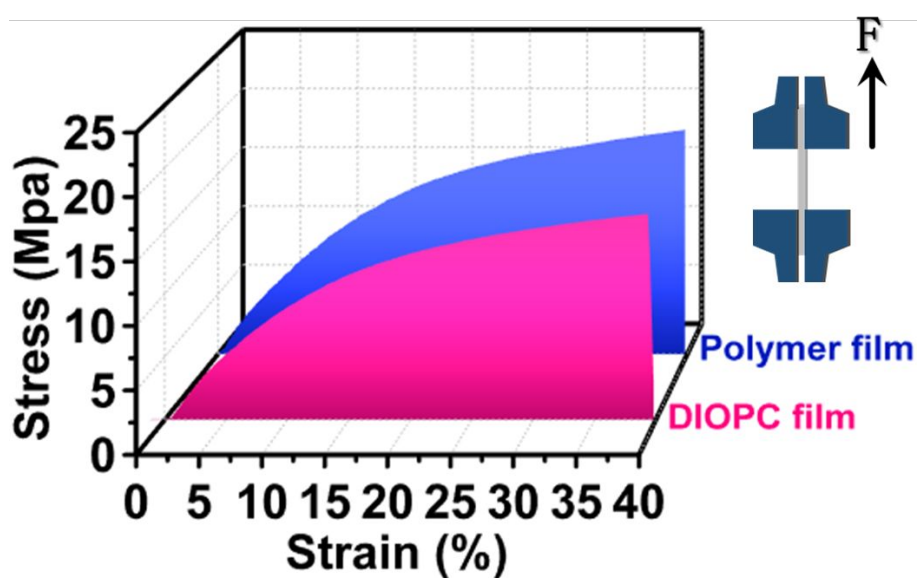


**Figure S7.** Tensile strain curves of the pure polymer film and the DIOPC film; the inset is the schematic diagram of the tensile test.

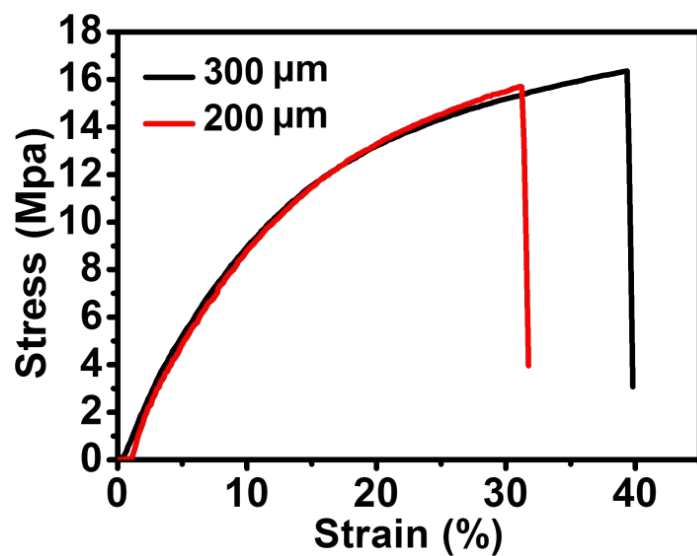


**Figure S8.** Tensile strain curves of the DIOPC film prepared with different thicknesses.

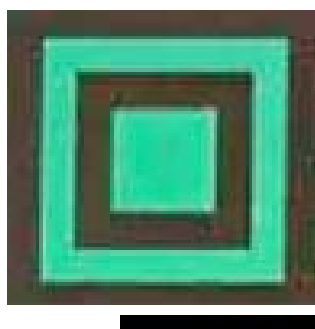


**Figure S9.** The pattern obtained by using the Fiber Laser Marking Machine. The scale bar in the inset is 0.5 cm.

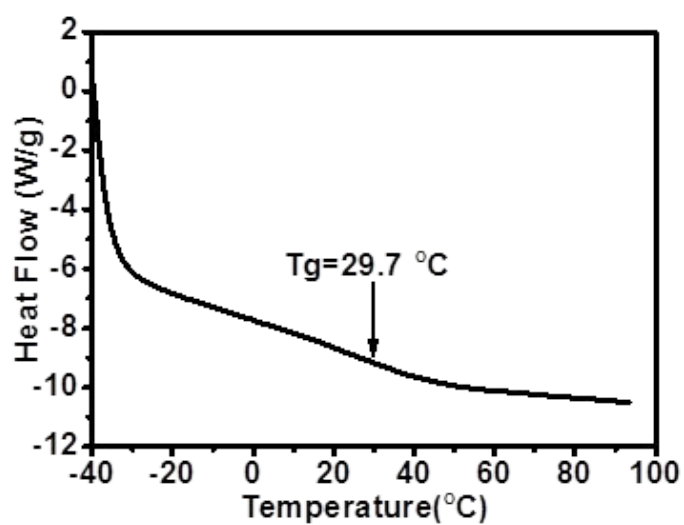


**Figure S10.** The DSC curve of the prepared BDIOPC film.



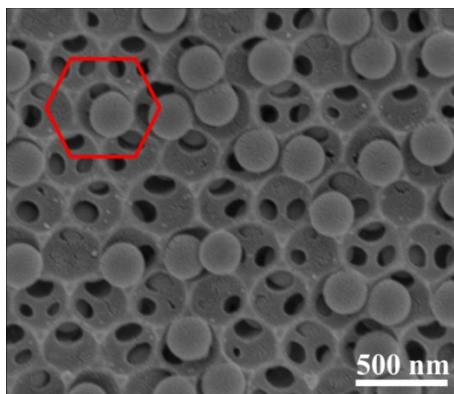


**Figure S11.** Cross-sectional SEM image of the close-up view of the top layer.

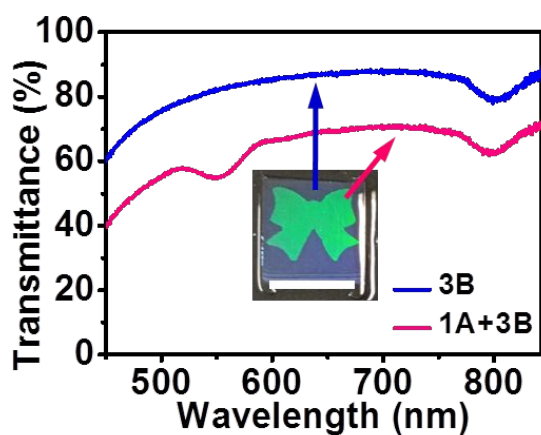


**Figure S12.** Transmission spectra of the prepared BDIOPC film sample wiped with ethanol both the top layer and bottom layer (3B represents the single top layer at 3B thickness and 1A+3B represents the whole BDIOPC film); inset is the photo of the BDIOPC film with a bowknot and the scale bar in the inset is 2 cm.

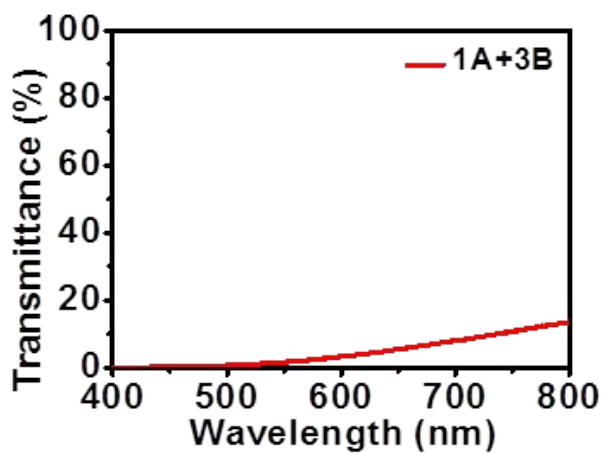


**Figure S13.** Transmission spectrum of the prepared BDIOPC film.

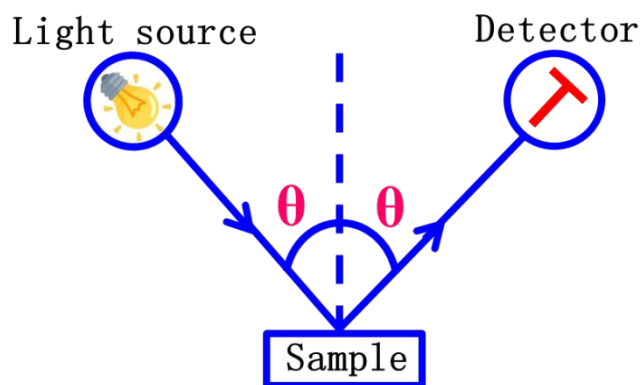


**Figure S14.** The diagram of the specular reflection model.

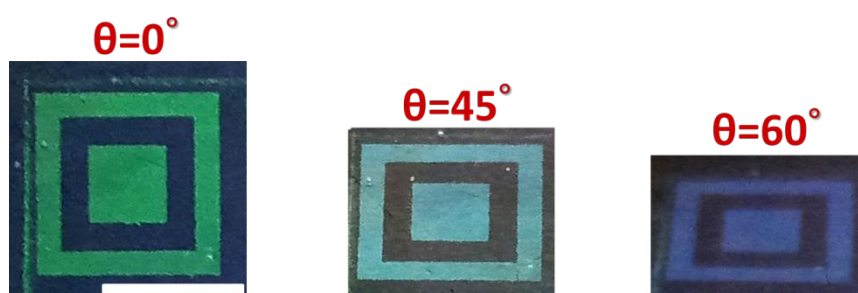


**Figure S15.** Digital photos of the patterned BDIOPC film at different viewing angles after the ethanol response. The scale bar in the inset is 0.5 cm.

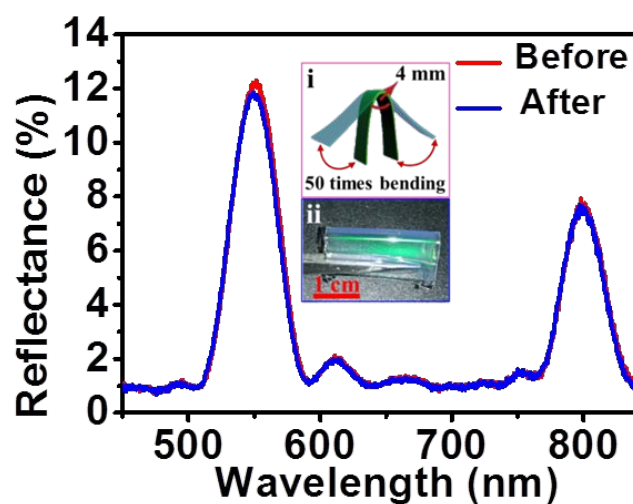


**Figure S16.** Reflectance spectra of the prepared BDIOPC film before and after 50 bending tests; insets are the schematic of the bending test and the obtained digital photo of the bent BDIOPC film.

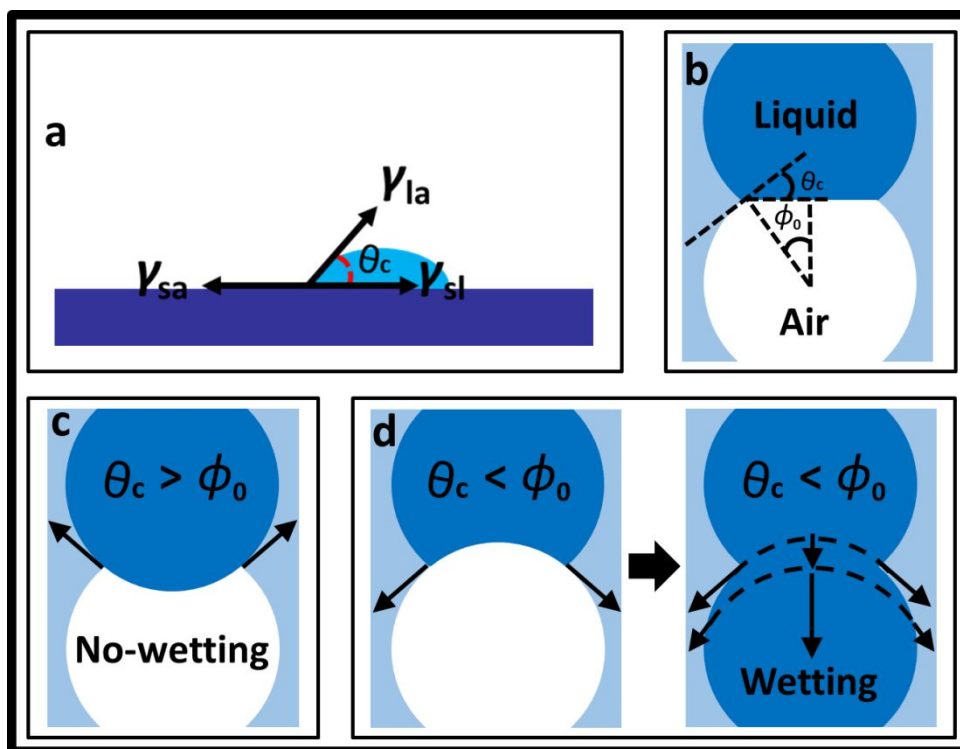


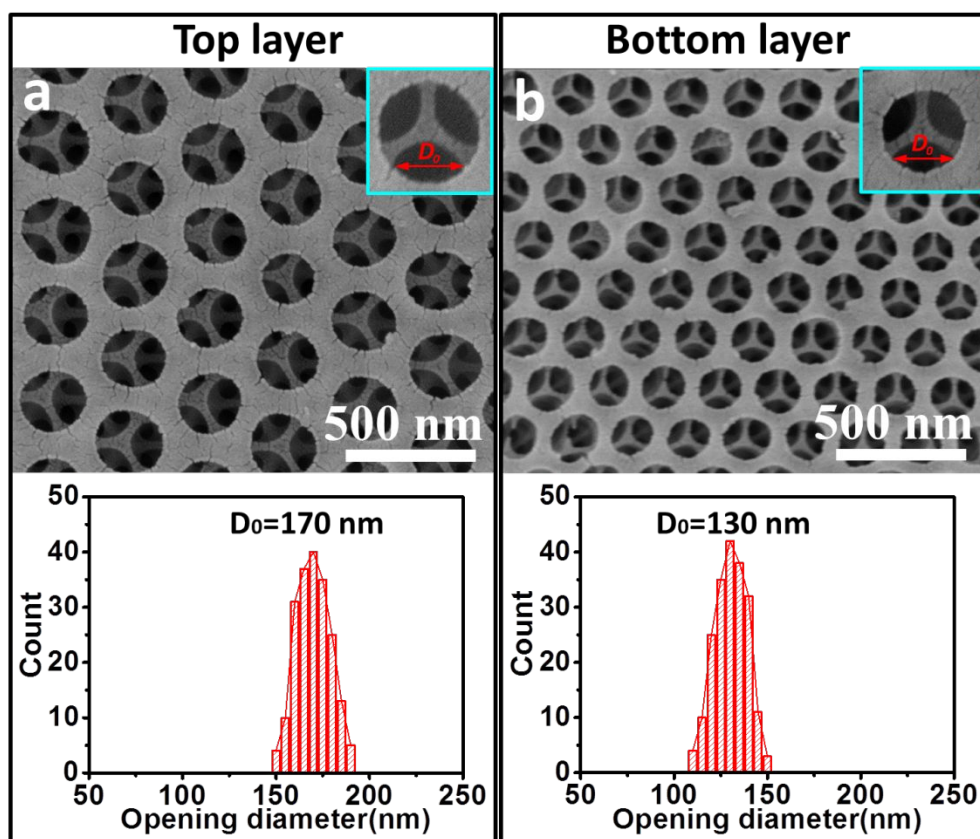
**Figure S17.** (a) Schematic diagram of the contact angle of the liquid on the solid surface ( $\gamma_{sa} - \gamma_{sl} = \gamma_{la} \cos\theta_c$ , where  $\theta_c$  is the measured contact angle,  $\gamma_{sa}$ ,  $\gamma_{sl}$ , and  $\gamma_{la}$  are the solid-air, solid-liquid, and liquid-air surface tensions, respectively). (b) Schematic of the liquid front propagating at the neck of two connected balls of the inverse opal structure (where  $\theta_c$  indicates the measured contact angle of the liquid on the inverse opal structure surface,  $\phi_0$  is the azimuthal angle). (c) Schematic illustration of the no-wetting state (if  $\theta_c > \phi_0$ , no infiltration occurs). (d) Schematic illustration of the wetting state (if  $\theta_c < \phi_0$ , infiltration occurs).

	Top layer									
Ethanol concentrations (v/v%)	0	5	10	15	20	25	27.5	30	32.5	100
Contact angle	50.2°	42.8°	38.0°	34.1°	31.3°	26.9°	23.0°	18.6°	13.5°	1.5°

	Bottom layer									
Ethanol concentrations (v/v%)	0	5	10	15	20	22.5	25	27.5	30	100
Contact angle	47.0°	40.1°	36.2°	33.0°	28.9°	26.9°	25.5°	20.0°	16.0°	1.2°

**Figure S18.** Contact angles of different concentrations of ethanol on the surface of the obtained BDIOPC film.



**Figure S19.** SEM images of the top view of the treated BDIOPC film with toluene (a, the top layer; b, the bottom layer; the PS spheres inside the pores of the BDIOPC film were removed) and corresponding opening diameter distribution diagrams.

## References

- (1) Aguirre, C. I.; Reguera, E.; Stein, A. Tunable Colors in Opals and Inverse Opal Photonic Crystals. *Adv. Funct. Mater.* **2010**, *20*, 2565-2578.
- (2) Zhong, K.; Song, K.; Clays, K. Hollow Spheres: Crucial Building Blocks for Novel Nanostructures and Nanophotonics. *Nanophotonics*. **2018**, *7*, 693-713.